Ocean Dynamics (2004) 54: 570–576
DOI 10.1007/s10236-004-0098-3

Jochen Horstmann · Wolfgang Koch · Susanne Lehner

Ocean wind fields retrieved from the advanced synthetic aperture radar aboard ENVISAT

Received: 27 November 2003 / Accepted: 15 December 2003

Abstract In this paper an algorithm is presented which enables high-resolution ocean surface wind fields to be retrieved from the advanced synthetic aperture radar (ASAR) data acquired by the European remote sensing satellite ENVISAT. Wind directions are extracted from wind-induced streaks that are visible in ASAR images at scales above 200 m and that are approximately in line with the mean surface wind direction. Wind speeds are derived from the normalized radar cross section (NRCS) and image geometry of the calibrated ASAR images, together with the local ASAR-retrieved wind direction. Therefore the empirical C-band model CMOD4, which describes the dependency of the NRCS on wind and image geometry, is used. CMOD4 is a semi-empirical model, which was originally developed for the scatterometer of the European remote sensing satellites ERS-1 and 2 operating at C-band with vertical polarization. Consequently, CMOD4 requires modification when applied to ASAR images that were acquired with horizontal polarization in transmitting and receiving. This is performed by considering the polarization ratio of the NRCS. To demonstrate the applicability of the algorithm, wind fields were computed from several ENVISAT ASAR images of the North Sea and compared to atmospheric model results of the German weather service.

Keywords Ocean winds · Satellite Remote sensing · Synthetic aperture radar · Spatial Wind Measurements · ENVISAT

Responsible Editor: Jörg-Olaf Wolff

J. Horstmann (✉) · W. Koch
GKSS Research Center, Institute for Coastal Research,
Max-Planck-Str. 1, 21502 Geesthacht, Germany
e-mail: horstmann@gkss.de

S. Lehner
German Space Agency, Remote Sensing Technology Institute,
Oberpfaffenhofen, 82234 Wessling, Germany

1 Introduction

Today, several scatterometers (SCATs) are in orbit, which enable ocean surface wind fields to be measured with a resolution of up to 25 km on a global and operational basis independent of daylight and cloudiness, e.g. QuikSCAT. All these SCATs were originally not designed to measure high-resolution wind fields and therefore make it difficult to measure the highly spatially variable winds, especially in coastal areas. However, satellite-borne synthetic aperture radar (SAR) instruments enable the ocean surface to be imaged with a very high resolution of up to ~30 m and a large spatial coverage of up to 500 km swath widths. This enables imaging with one single swath nearly the entire North or Baltic Sea. Figure 1 shows a 25×20-km subimage of the SAR aboard ERS-2 acquired at the west coast of Norway near to Bergen on the 13. February, 2000. In the open waters a wave system can be seen which is approaching the Norwegian coast from the west and which is refracted by the islands. Behind the island, streak-like structures oriented in east–west direction are visible, which are induced by the wind shadowing of the islands as well as the local variability of the wind field. The high-resolution and large spatial coverage of spaceborne SAR data make them a very valuable tool, especially in coastal regions, for measuring geophysical parameters such as ocean surface winds, waves and sea ice.

Since the launching of the European remote sensing satellites ERS-1, ERS-2, and ENVISAT, as well as the Canadian satellite RADARSAT-1, SAR images have been acquired over the oceans on a continuous basis. The advanced SAR (ASAR) aboard the European satellite ENVISAT operates in the C band (5.34 GHz) and, in contrast to the ERS-1/2 and RADARSAT-1 satellites, at both vertical (VV) and, horizontal (HH) polarization in transmitting and receiving. All sensors acquire SAR data at moderate incidence angles between 15° and 50°. For this electromagnetic wavelength

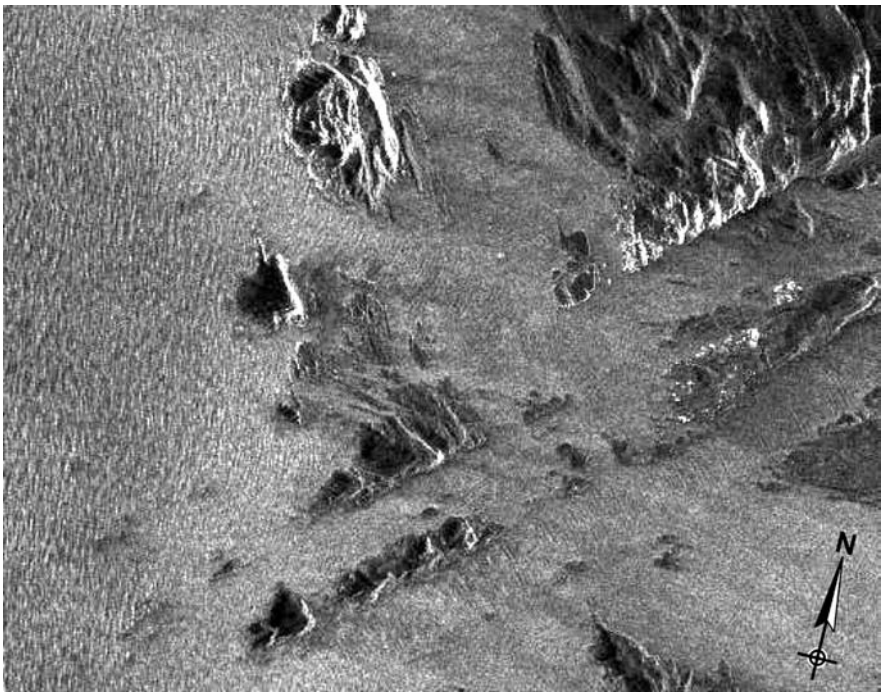

Fig. 1 Synthetic aperture radar (SAR) subimage (25×20 km) of the west coast of Norway near Bergen. The image was acquired on 13. February, 2000, by the SAR aboard the European remote sensing satellite ERS-2

and range of incidence angles the backscatter of the ocean surface is primarily caused by the small-scale surface roughness (5 to 10-cm scales), which is strongly influenced by the local wind field and therefore allows the backscatter to be empirically related to the wind.

In the past years much effort has been undertaken to develop algorithms for derivation of wind vectors from SAR images. The wind direction can be retrieved from the direction of wind-induced streaks, which can be retrieved either in the spectral domain (Gerling 1986; Vachon and Dobson 1996; Fetterer et al. 1998; Lehner et al. 1998; Horstmann et al. 2000a) or in the spatial domain (Horstmann et al. 2002; Koch 2004). The wind speed is derived from the intensity of the SAR image, using semi-empirical C-band models for VV polarization (Fetterer et al. 1998; Lehner et al. 1998; Horstmann et al. 2000a, 2003). If the SAR is operating at HH polarization these models have been extended (Horstmann et al. 2000b; Thompson and Beal 2000; Vachon and Dobson 2000; Horstmann et al. 2002; Wackerman et al. 2002).

In this paper an algorithm for wind field retrieval from C-band SAR data is introduced, and for the first time wind fields are retrieved from ENVISAT ASAR data. To show the applicability of the algorithm ENVISAT ASAR-retrieved wind fields in the North Sea are compared to results of the numerical atmospheric model of the German weather service (DWD).

The paper is organized as follows: in Section 2 the ENVISAT ASAR is described. In Section 3 a description of the SAR wind-retrieval method is given. In Section 4 ASAR-retrieved wind fields are compared to model results of the DWD.

2 Utilized ENVISAT ASAR data

The advanced synthetic aperture rader (ASAR) aboard the European satellite ENVISAT operates at C-band (5.34 GHz) in a sun-synchronous polar orbit. ENVISAT's orbit is at a height of ~800 km, which results in a 35-day repeat cycle with an orbital period of 100 min. For this study ASAR data were acquired in the ScanSAR wide-swath mode, which enables up to 30 min per orbit be acquired. ScanSAR images are generated by scanning the incidence angle and subsequently synthesizing images for five different subswaths at incidence angles between approximately 15° and 45.2°. The ScanSAR wide-swath mode enables a ~400 km wide swath to be imaged with a spatial resolution of ~150 m and a pixel size of 75 m. For the following study ASAR data were acquired at either HH or VV polarization in transmitting and receiving. Prior to the wind-speed retrieval, the ASAR data have to be absolutely calibrated to normalized radar cross section (NRCS) (ASAR team 2003).

3 SAR wind retrieval

Wind retrieval from SAR data is a two-step process. In the first step wind directions are extracted from wind-induced streaks visible in the SAR image. These wind directions are used in the second step, where wind speeds are derived from the NRCSs of the SAR data under consideration of the wind direction and SAR imaging geometry.

3.1 SAR wind-direction retrieval

The most popular method for SAR wind-direction retrieval is based on the imaging of structures such as marine atmospheric boundary layer (MABL) rolls (Alpers and Brümmer 1994), which have a typical spacing of 2 to 10 km. The orientation of the MABL rolls is between the direction of the mean surface wind and the geostrophic wind above the boundary layer and varies between 20° to the left and 30° to the right of the geostrophic wind (Etling and Brown 1993). Nevertheless, wind-induced streaks observed in SAR imagery were compared with in situ wind observations (Gerling 1986; Vachon and Dobson 1996; Fetterer et al. 1998; Lehner et al. 1998). All report average wind-row directions within 15° of in situ surface wind directions with possible errors that were much larger. The large errors are most likely due to other atmospheric features, which are not aligned with the surface wind direction, but are also imaged by the SAR at these scales, e.g. see waves and inflection point instabilities. Studies by Horstmann et al. (2002) have shown that wind-induced streaks that are oriented in wind direction are often detected in scales between 200 and 1600 m, which are most likely associated with wind streaks (Drobinski and Foster 2003) and seldom to MABL rolls. Their comparison of SAR-retrieved wind direction at scales above 200 m with an atmospheric model resulted in a root mean square error of ~22°. Also studies of Dankert et al. (2003), utilizing tower-based high-resolution real aperture radar (RAR) imagery, have shown that wind-induced streaks at scales between 50 to 1500 m are very well aligned with the mean surface wind. Their comparison of 3272 radar image sequences acquired over a 6 month period, to in situ wind measurements showed that the streaks are very well aligned with the surface wind directions (root mean square error of 14.2°). Therefore, in the following, the linear features visible in the SAR images are assumed to be aligned with the mean surface wind direction. Furthermore, the results of Dankert et al. (2003) encourage focusing on the smallest possible scales which can be utilized from space-borne SAR.

Two methods have been developed in the past to extract the orientation of wind-induced streaks. The first method searches for the dominant wind-streak direction in the wavenumber domain (Lehner et al. 1998) and is referred to as the fast-Fourier transformation method (FFT method). Therefore, SAR subimages are transformed into the wavenumber domain where a regression analysis is performed on the energy densities for wavelengths between 500 and 1800 m. The main spectral energy is located perpendicular to the orientation of the streaks, giving the wind direction with a 180° ambiguity. In the second method the wind direction is defined as normal to the local gradients derived from smoothed amplitude images (Horstmann et al. 2002; Koch 2004). In the following, this method is referred as the local gradient method (LG method). In a first step the SAR images are smoothed and reduced to a pixel size of 100, 200 and 400 m, representing scales above 200 m. From these pixels the local directions, defined by the normal to the local gradient, are computed with a 180° ambiguity. In a next step all pixels that are effected by non-wind-induced features, e.g. land, surface slicks, sea ice etc., are masked. Therefore, land masks and SAR image filters, which are described by Koch (2004), are applied. Finally, from all the resulting directions only the most frequent directions in a predefined grid cell are selected. The wind directions resulting from the 100, 200 and 400 m pixel sizes vary typically by only a few degree, except for cases where additional features are present in the SAR image, e.g. see waves. The 180° directional ambiguity can be removed if wind shadowing is present, which is often visible in the lee of coastlines. If such features are not present in the image, other sources, e.g. atmospheric models or in situ measurements, have to be considered.

3.2 SAR wind-speed retrieval

For the wind-speed retrieval a model function relating the NRCS of the ocean surface to the local near-surface wind speed, wind direction versus antenna-look direction and incidence angle is utilized. This function is dependent on radar frequency and polarization. In the case of the ERS-1 SCAT operating at C-band with VV polarization, several empirical functions have been developed, of which the CMOD4 (Stoffelen and Anderson 1997) and CMOD_IFR2 (Quilfen et al. 1998) are the most commonly used, and the CMOD5 (Hersbach 2003) the most recently developed. It has been shown that these functions are applicable for wind-speed retrieval from VV polarized SAR images (Vachon and Dobson 1996; Lehner at al. 1998; Horstmann et al. 2003). Comparison indicate that the CMOD4 model function is the best choice for low to moderate wind speeds (J. Horstmann and W. Koch, 2004). For wind-speed retrieval from C-band HH polarized SAR images, no similar well-developed model exists. So that a hybrid model function is applied that consists of the above models, e.g. CMOD4, and a C-band polarization ratio (PR) (Horstmann et at. 2000b; Thompson and Beal 2000; Vachon and Dobson 2000), defined as:

$$\mathrm{PR} = \frac{\sigma_0^{HH}}{\sigma_0^{VV}}, \tag{1}$$

where σ_0^{HH} and σ_0^{VV} are the HH and VV polarized NRCS, respectively. So far, the PR is not well known, and several different PRs are suggested in the literature (Elfouhaily 1997; Thompson et al. 1998).

The PR proposed by Thompson et al. (1998) neglects wind-speed and wind-direction dependency and is given by:

$$\mathrm{PR} = \frac{(1 + \alpha \tan^2 \theta)^2}{(1 + 2\tan^2 \theta)^2}, \tag{2}$$

where α is a constant and set to 0.6, fitting the measurements of Unal et al. (1991). This form is closely related to theoretical forms of the PR, where $\alpha = 0$ gives the theoretical PR for Bragg Scattering and $\alpha = 2$ results in Kirchhoff scattering. Several different values for α have been suggested in the past considering RADARSAT-1 SAR data; they vary between 0.4 and 1.2 (Horstmann et al. 2000b; Vachon an Dobson 2000; Monaldo et al. 2002). Comparisons of RADARSAT-1 SAR data of different SAR–processing facilities showed that the different findings of α are most likely due to the different calibrations of RADARSAT-1 SAR data.

In Fig. 2 an ERS-1 SAR image acquired on the 8. September 1995 of the Danish island Bornholm in the Pomeranian Bay of the Baltic Sea is depicted. Superimposed on the image are the wind vectors (black arrows) resulting from the LG method and the CMOD4 model as well as the wind directions resulting from the FFT method. The directional ambiguity of the wind directions can be removed due to the visible wind-shadowing effects of Bornholm. The easterly wind directions and wind speeds $\sim$8 ms^{-1} agree well with the observations from weather charts. Comparison of the LG method with the FFT method show in some places significant differences and in all cases the LG method shows the more realistic results. For this reason, the LG method will be used in this study to retrieve wind directions from the ENVISAT ASAR imagery.

4 Comparison of SAR wind fields with an atmospheric model

To show the applicability of wind-field retrieval utilizing ENVISAT ASAR data, 12 ScanSAR image datasets acquired over the North Sea were considered. Of these 12 ScanSAR images, 6 were acquired at VV and 6 at HH polarization, respectively. For comparison with the SAR-derived wind fields, results from the DWD model were utilized, which represent 6 h analyzed wind fields and were interpolated to the SAR acquisition time. The SAR wind fields were retrieved from the area corresponding to the grid cell in the DWD model output, resulting in an average grid cell size of approximately 45×75 km. Prior to the wind retrieval, all pixels representing land and artefacts not due to the local wind, such as current shear and surface slicks, are masked. This process includes the assessment of digital maps and thresholds resulting from the wind-retrieval algorithm (Koch 2004). The directional ambiguities of the SAR-retrieved wind directions were removed by considering wind shadowing as well as weather charts. The resulting wind direction, mean NRCS and mean incidence angle of each grid cell are taken as input to the wind-speed retrieval algorithm for VV or HH polarization, respectively.

Figure 3 shows an ENVISAT ASAR image of the southern North Sea and Strait of Dover acquired on December 1, 2002 at 10:02 h UTC in the ScanSAR mode with VV polarization in transmitting and receiving. Superimposed on the image are the wind vectors as retrieved from the SAR image (white arrows) and resulting from the DWD model (black arrows) . The wind direction ambiguities could be removed due to the wind shadowing, which is especially visible on the north coast of Germany. The contrast-enhanced cutout (lower right of Fig. 3) shows the coastal wind shadowing in more detail. In most parts of the image the SAR-retrieved winds agree very well with the DWD model results in both magnitude and direction.

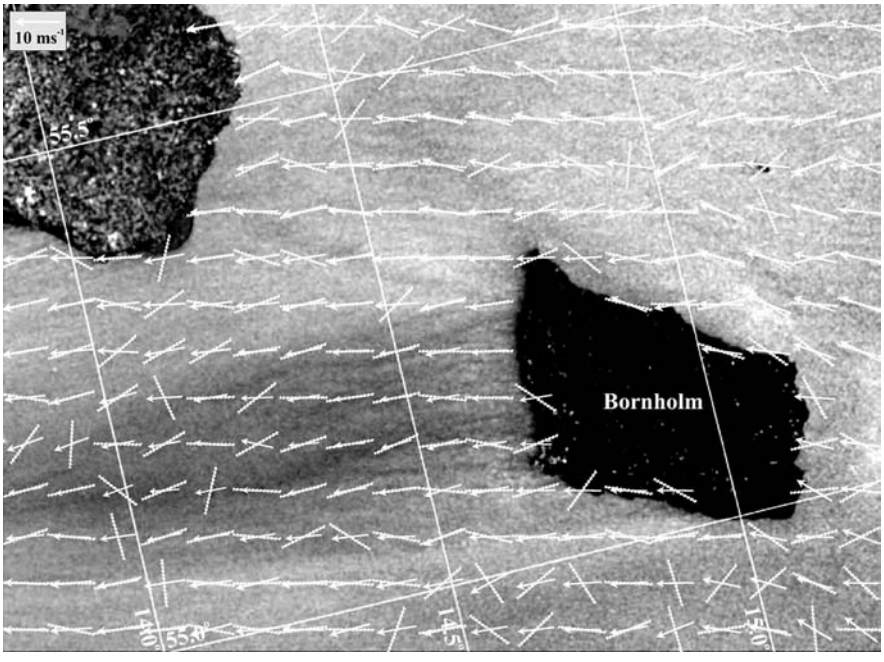

Fig. 2 ERS-1 SAR subimage of Bornholm situated in the Pomeranian Bay of the Baltic Sea. The image was acquired on the 8. September 1995 at 10:02h UTC during moderate easterly winds. The *yellow superimposed wind vectors* were retrieved using the local gradient method for wind directions and the CMOD4 model for wind speeds. The *dotted bars* represent the wind directions resulting from the fast-Fourier transform method

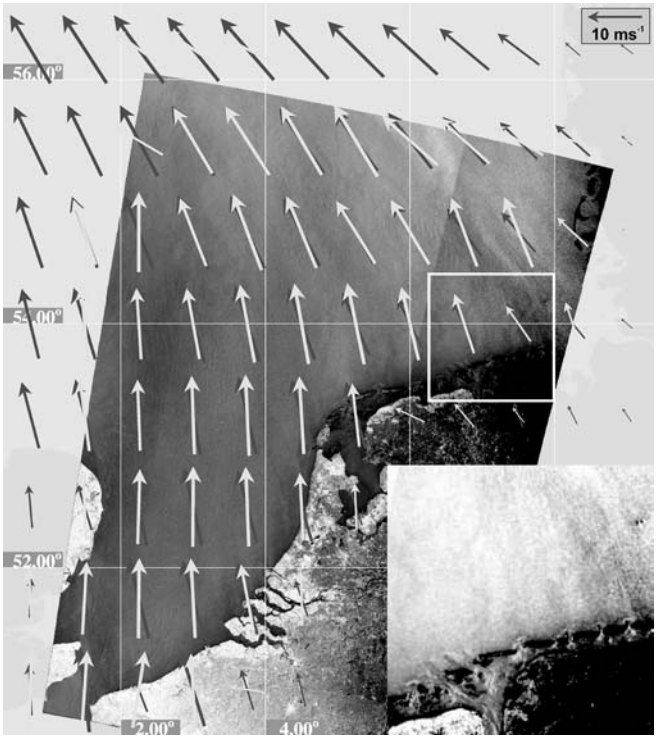

Fig. 3 ENVISAT ASAR image acquired on 1. December, 2002 with vertical (VV) polarization in transmit and receive, showing the southwest of the North Sea. *White arrows* represent the wind vectors resulting from the SAR data and *black arrows* those from the model of the German weather service (DWD). The contrast-enhanced cutout (*lower right*) shows the wind shadowing due to the German coast

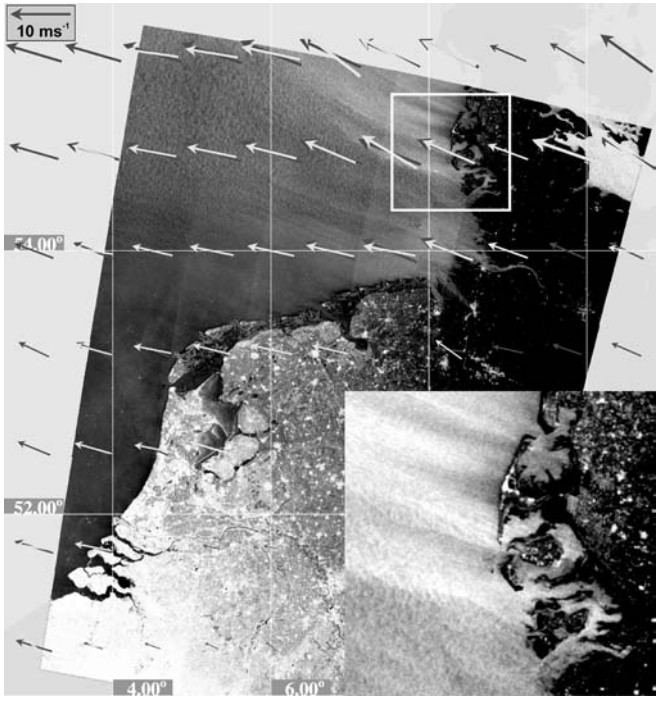

Fig. 4 As Fig. 3, however acquired on 14. December, 2002 with horizontal (HH) polarization in transmit and receive, showing the southern North Sea

In Fig. 4 an ENVISAT ASAR image of the southern North Sea is depicted, which was acquired on December 14, 2002, at 09:53 h UTC in the ScanSAR mode with HH polarization in transmitting and receiving. Again, the wind-direction ambiguities could be removed due to the wind shadowing visible in the SAR image, especially on the west coast of Germany, as can be seen in the contrast-enhanced cutout of Fig. 4. The wind directions agree very well in most parts of the area considered; however, wind speeds are slightly underestimated in most parts of the image.

In a next step all SAR-retrieved wind vectors were compared to the DWD model winds. The resulting scatterplot is shown in Fig. 5a, where DWD model wind directions are plotted versus SAR-retrieved wind directions. The resulting correlation in wind direction is 0.95 with a bias of −6.1° and a standard deviation of 18.9°. This is very similar to the wind-direction error of 15° achieved by the SCAT aboard ERS (Quilfen et al. 1998). Comparison of DWD model wind speeds to SAR-retrieved wind fields utilizing the SAR-retrieved wind directions (Fig. 5b) resulted in a correlation of 0.87 with a negligible bias and a standard deviation of 2.5 ms^{-1}. Overall, the comparison of DWD- and SAR-retrieved wind speeds do not show a good consistency, which is most likely due to the resolution of the DWD model,

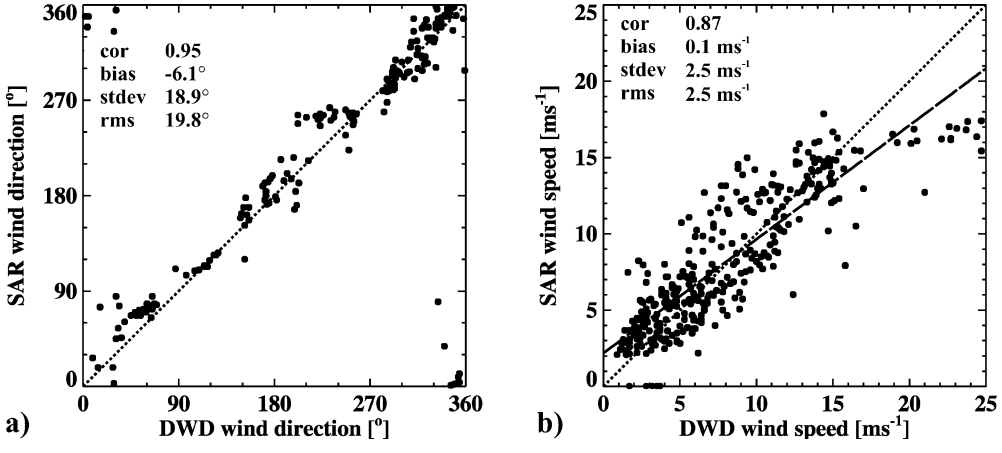

Fig. 5a,b Scatterplots giving the comparison of results from the DWD model versus colocated results from ENVISAT ASAR images. Results of wind directions are given in **a** and wind speeds in **b**

which is too coarse for resolving wind shadowing as well as other small-scale features that occur especially near to the coasts. Also the excellent consistency of wind speeds retrieved from colocated SAR and the European Centre for Medium-Range Weather Forecast (ECMWF) model runs (showing a standard deviation of 1.6 m s^{-1}) (Horstmann et al. 2003) supports this assumption.

It was already stated that wind speeds retrieved from the ScanSAR image shown in Fig. 4 are slightly lower than the DWD model results. This could be due to too large a choice of α in Eq.(2), which leads to lower SAR wind speeds. However, the statistics from the wind-speed comparison between DWD model results and ScanSAR HH polarized results show no significant bias and therefore no need to change α.

5 Conclusions and outlook

An algorithm for retrieval of wind fields from SAR imagery acquired at C band with either VV or HH polarization in transmitting and receiving has been introduced. Wind-field retrieval is a two-step process: in the first step, wind directions are extracted from wind-induced streaks imaged by the SAR at scales above 200 m. These streaks are assumed to be aligned wind direction and are extracted by determining the local gradient, which is perpendicular to the streak orientation. To resolve the 180° ambiguity, wind shadowing visible at the coast was taken into account. In the second step, wind speeds were retrieved using an empirical model that gives the dependency of the NRCS on wind speed, wind direction and incidence angle. The model was developed for the ERS-1 SCAT operating at C-band with VV polarization, and was extended to HH polarization by considering an incidence-angle-dependent polarization ratio.

Comparison of ENVISAT ASAR-retrieved winds with colocated results of the atmospheric model of the DWD showed promising results for wind directions. However, in the case of wind speeds, the standard deviation was 2.5 ms^{-1}, which is most likely due to the too-coarse model resolution that cannot resolve the strong wind-speed variability near to the coasts. For wind-speed retrieval from HH polarized ASAR data, the hybrid model function consisting of CMOD4 and an incidence-dependent polarization ratio with $\alpha = 1$ is a good choice. However, an in-depth analysis investigating polarization ratio dependencies on the wind speed and direction still has to be undertaken.

Acknowledgements The authors were supported by the German Bundesministerium für Bildung und Forschung (BMBF) in the framework of the project. 'A new perspective of the Ocean ENVISAT Oceanography' (ENVOC). The ENVISAT ASAR data were kindly made available by the European Space Agency in the framework of the ENVISAT Project AO-ID 220, Biological and geophysical parameters from synthetic aperture radar over the ocean (BIGPASO).

References

Alpers W, Brümmer B (1994) Atomospheric boundary layer rolls observed by the synthetic aperture radar aboard the ERS-1 satellite. J Geophys Res 99: 12613–12621

ASAR Team (2003) Absolute calibration of ASAR level 1 products generated with PF-ASAR. Technical note, issue 1, rev. 2, envi-clvl-eopg-tn-03-0010, ESA publication division, ESTEC, Noordwijk, The Netherlands

Dankert H, Horstmann J, Rosenthal W (2003) Ocean winds fields retrieved from radar-image sequences. J Geophys Res 108(C11): 3352, DOI 10.1029/2003JC002056.

Drobinski P, Foster RC (2003) On the origin of near-surface streaks in the neutrally stratified planetary boundary layer. Bound-Layer Meteorol 108(2): 247–256

Elfouhaily TM (1997) Physical modeling of electro-magnetic backscatter from the ocean surface; application to retrieval of wind fields and wind stress by remote sensing of the marine atmospheric boundary layer, PhD Thesis, Travail de recherche effectué ausein Départment d'Océanographie Spatiale de l'Institut Français de Recherche pour l'Exploitation de la Mer (IFREMER), Brest, France

Etling D, Brown RA (1993) Roll vortices in the planetary boundary layer: a review. Boundary-Layer Meteorol 18: 215–248

Fetterer F, Gineris D, Wackerman C (1998) Validating a scatterometer wind algorithm for ERS-1 SAR. IEEE Trans Geosci Remote Sens 36(2): 476–492

Gerling TG (1986) Structure of the surface wind field from Seasat SAR. J Geophys Res 91: 2308–2320

Hersbach H (2003) CMOD5 an improved geophysical model function for ERS C-band scatterometry. International report, European Centre for Medium-Range Weather Forecast

Koch W (2004) Directional analysis of SAR images aiming at wind direction. IEEE Trans Geosci Remote Sens 42(4): 702–710

Horstmann J, Lehner S, Koch W, Tonboe R (2000a) Computation of wind vectors over the ocean using spaceborne synthetic aperture radar. John Hopkins APL Tech Dig 21(1): 100–107

Horstmann J, Koch W, Lehner S, Tonboe R (2000b) Wind retrieval over the ocean using synthetic aperture radar with C-band HH polarization. IEEE Trans Geosci Remote Sens 38(5): 2122–2131

Horstmann J, Koch W, Lehner S, Tonboe R (2002) Ocean winds from RADARSAT-1 ScanSAR. Can J Remote Sens 28(3): 524–533

Horstmann J, Schiller H, Schulz-Stellenfleth J, Lehner S (2003) "Global wind speed retrieval from SAR". IEEE Trans Geosci Remote Sens 41(10): 2277–2286

Horstmann J, Koch W (2004) "High resolution ocean surface wind fields retrieval from spaceborne synthetic aperture radars operating at C-band", ESA SP-Series (in press)

Lehner S, Horstmann J, Koch W, Rosenthal W (1998) Mesoscale wind measurements using recalibrated ERS SAR images. J Geophys Res 103: 7847–7856, 1998

Monaldo F, Thompson DR, Beal RC, Pichel W, Clemente-Colon P (2002) Comparison of SAR-derived wind speed with model predictions and ocean buoy measurements. IEEE Trans Geosci Remote Sens 39(12): 2587–2600

Quilfen Y, Chapron B, Elfouhaily TM, Katsaros K, Tourandre J (1998) Observation of tropical cyclones by high-resolution scatterometry. J Geophys Res 103: 7767–7786

Stoffelen A, Anderson D (1997) Scatterometer data interpretation: estimation and validation of the transfer function CMOD4. J Geophys Res 102: 5767–5780

Thompson DR, Beal RC (2000) Mapping of mesoscale and submesoscale wind fields using synthetic aperture radar. John Hopkins APL Tech Dig 21(1): 58–67

Thompson DR, Elfouhaily TM, Chapron B (1998) Polarization ratio for microwave backscattering from the ocean surface at low to moderate incidence angles. In: Proc Int Geosci Remote Sens Symp. 1998, Seattle, USA

Unal CMH, Snoeij P, Swart PJF (1991) The polarization-dependent relation between radar backscatter from the ocean surface and surface wind vectors at frequencies between 1 and 18 GHz. IEEE Trans Geosci Remote Sens 29: 621–626

Vachon PW, Dobson FW (1996) Validation of wind vector retrieval from ERS-1 SAR images over the ocean. Global Atmos Ocean Syst 5: 177–187

Vachon PW, Dobson FW (2000) Wind retrieval from RADARSAT SAR images: selection of a suitable C-band HH polarization wind-retrieval model. Can J Remote Sens 26(4): 306–313

Wackerman C, Clemente-Colon P, Pichel W, Li X (2002) A two-scale model to predict C-band VV and HH normalized radar cross-section values over the ocean. Can J Remote Sens 28(3): 367–384